

# Effect of Interlayer Potential on Mechanical Deformation of Multiwalled Carbon Nanotubes

Dong Qian,<sup>a</sup> Wing Kam Liu,<sup>b,\*</sup> Shekhar Subramoney,<sup>c</sup> and Rodney S. Ruoff<sup>b,\*</sup>

<sup>a</sup>Department of Mechanical, Industrial and Nuclear Engineering, University of Cincinnati, Cincinnati, Ohio, USA

<sup>b</sup>Department of Mechanical Engineering, Northwestern University, Evanston, Illinois, USA

<sup>c</sup>DuPont Central Research and Development, Experimental Station, Wilmington, Delaware, USA

A study on the modeling and simulation of interlayer interaction in the multiwalled carbon nanotube (MWCNT) system is presented. We use an interlayer Morse potential previously developed from a local density approximation (LDA) treatment of a bilayer of graphite. We have fit this Morse potential to experimental high-pressure compressibility data for graphite and to a more extensive LDA equation of state (EOS) for graphite, and excellent agreement is observed. We employ this potential to treat the interlayer mechanics of MWCNTs, where the MWCNT is so highly deformed that interlayer separation well below  $\sim 0.34$  nm, such as down to  $\sim 0.26$  nm, is occurring. This, to our knowledge, is the first treatment that attempts to account for deformations that have the layers approaching each other at very high local (interlayer) stress levels. Since evaluating the interlayer potential for a large MWCNT system is computationally intensive, a continuum simulation approach is proposed that saves on computational time and thus on cost. Comparisons with experimental results of buckled and highly kinked MWCNTs are presented.

**Keywords:** Nanotube, Interlayer Potential, LJ Potential, Morse Potential, Beam Theory.

## 1. INTRODUCTION

Multiwalled carbon nanotubes (MWCNTs) were the first carbon nanotubes to be discovered.<sup>1</sup> The structure of MWCNTs is a Russian doll-like structure (nested shells), as revealed from transmission electron microscopy (TEM) studies. The interlayer spacing is approximately  $\sim 0.34$  nm,<sup>2,3</sup> close to the interlayer separation of graphite, 0.335 nm. The interlayer interaction is of the weak van der Waals type, yielding a weak interlayer rigidity and strength. For instance, in the experimental study of "shell-sliding,"<sup>4</sup> it was found that the shear strength between the outermost shell and the neighboring inner shell was 0.08 MPa and 0.3 MPa for two different MWCNTs. An experiment by Cumings and Zettl<sup>5</sup> also suggested that the contact between layers in MWCNTs is almost frictionless, thus suggesting their use as a nano-bearing system. This weak load transfer between the MWCNT layers could be a major obstacle for their effective use in mechanical applications, particularly for the case of tensile loading.

Exceptional tensile strength of carbon nanotubes has been measured in a few experiments. But before this tensile strength stress value is reached, structural instability for tubes under compression, bending, or torsion can easily take place. A comprehensive review of this topic is

given by Qian et al.<sup>6</sup> For instance, buckling due to bending and torsion was demonstrated in Refs. 7–9. In the case of bending, the buckling pattern is characterized by the collapse of the cross section at some location along the tube. When MWCNTs collapse or buckle, the effect of interlayer interactions becomes important, as the neighboring shells may come into closer contact. One such example is the rippling mode in MWCNTs reported by Poncharal et al.,<sup>10</sup> which they related to the observed significant decrease in the (apparent) bending stiffness (of large-diameter MWCNTs) when fit to a continuum treatment of their resonant frequencies. Developing understanding of the details of the mechanics of buckling in this case is relevant for a host of prospective applications involving mechanical resonance or buckling under a mechanical load.

One important application that is closely related to this subject is the mechanical behavior of polymer materials reinforced by MWCNTs. In the past, Ruoff and his co-workers have developed an experimental method of observing the mechanical response of compressively loaded MWCNTs by TEM, by embedding the MWCNTs in a polymer material (polyvinylformal, known also by the trade name Formvar) that is sensitive to thermo loading. With this method, the mechanical deformation of both the polymer material and MWCNT can be captured. In general, when compressive loads are transferred from a polymer matrix to the MWCNT, it can still buckle in a

\*Authors to whom correspondence should be addressed.

confined environment. This is due partly to the fact that the polymer material typically has a much lower Young's modulus than does the embedded MWCNT; for example, the Young's modulus of Formvar is  $\sim 3$  GPa, whereas that of the NT is on the order of 1000 GPa. The polymer is much softer and so is the confinement. Effects such as buckling pattern, load transfer, confining pressure, and separation between MWCNT and matrix due to debonding must be correctly accounted for in the modeling of nanotube reinforced composites.

Another interesting by-product of local deformation is the enhanced chemical reactivity at the kink, which has been studied in both simulation and experiment.<sup>11</sup> This phenomenon, although it is not dealt with in this paper, can have a significant impact on the design of nano-electro-mechanical (NEM) devices, particularly for applications involving manipulations of nanometer-sized objects that might lead to high local deformation.

Compared with experiments, there are no reports on the simulation of the deformation of MWCNTs with many nested shells, to our knowledge. This is mainly due to the computational cost associated with evaluation of the interlayer potentials. The covalent bond potential has a shorter cut-off length. In contrast, evaluating the interlayer potential for one atom in a layer with the use of pairwise potentials can result in including the interactions with several hundred neighboring atoms. To overcome this difficulty, we propose the use of a continuum method. The computation of the interlayer interaction is first replaced with a surface integral, as suggested by Girifalco et al.<sup>12</sup> The corresponding molecular dynamics (MD) simulation is then replaced with a Galerkin approach, in which the atomic position is interpolated with the use of the concept of the mesh-free approximation.<sup>13</sup> This allows for a significant increase in the number of atoms in a system that can be modeled due to the reduction in the number of degrees of freedom.

We report here simulation results as well as experimental observations of the mechanical response of a MWCNT due to bending. The experimental observation of buckling modes is captured well in the simulation. To reveal the effect of interlayer interaction on local buckling, we compared our model with the widely used Lennard-Jones potential for carbon systems such as nanotubes and graphite. It is found that different interlayer potentials do not affect the onset of the buckling mode, but rather result in different post-buckling behavior. The Lennard-Jones (LJ) potential yields stiffer behavior than does the model we adapted.

## 2. INTERLAYER POTENTIALS

For carbon systems such as nanotubes and graphite, there are two major functional forms typically used in the empirical model for the interlayer potential: the inverse power model and the Morse function model. The LJ potential is

a very widely used inverse power model. For the carbon-carbon system, the LJ potential energy has been treated by Girifalco and Lad<sup>14</sup> and Girifalco<sup>15</sup> and is given as

$$\phi(r_i) = \frac{A}{\sigma^6} \left[ \frac{1}{2} y_0^6 \frac{1}{\left(\frac{r_i}{\sigma}\right)^{12}} - \frac{1}{\left(\frac{r_i}{\sigma}\right)^6} \right] \quad (1)$$

In Eq. (1),  $\sigma$  is the bond length,  $y_0$  is a dimensionless constant, and  $r_i$  is the distance between the  $i$ th atom pair. Two sets of parameters have been used: one for a graphite system<sup>14</sup> and the second for a  $C_{60}$  fcc crystal.<sup>15</sup> The converted parameters from the original data are given in Table I.

The Morse-type potential was derived by Wang et al.<sup>16</sup> for use in studying the  $(C_{60})$  fullerite solid under very high pressures and is based on LDA:

$$\phi(r_i) = D_e \left\{ \left( 1 - e^{-\beta(r_i - r_e)} \right)^2 - 1 \right\} + E_r e^{-\beta' r_i} \quad (2)$$

where  $D_e = 6.50 \times 10^{-3}$  eV is the equilibrium binding energy,  $E_r = 6.94 \times 10^{-3}$  eV is the hard-core repulsion energy, and  $r_e = 4.05$  Å is the equilibrium distance between two carbon atoms,  $\beta = 1.00/\text{Å}$  and  $\beta' = 4.00/\text{Å}$ .

For the parameters given in Table I, it is expected that the LJ potential is too repulsive because of the inverse power functional dependence for short interatomic distances. Indeed, the LJ potential poorly predicts the bulk modulus of fullerite, and the  $c$  axis compressibility of graphite, at high pressure. In a comparison study by Qian et al.,<sup>17</sup> it was found that the two LJ potentials yield much higher interatomic forces than does the Morse potential in the repulsive region, which further quantifies the difference. For example, the interatomic repulsive forces from LJ1, LJ2, and LDA are, respectively, 0.20 eV/Å, 0.29 eV/Å, and 0.069 eV/Å at an interatomic distance of 3.0 Å. This difference grows for shorter interatomic distances. On the other hand, the Morse potential gives a much lower binding energy than do the two LJ potentials in the attractive region. When the interatomic distance is 4.0 Å, the binding energies from LJ1, LJ2, and LDA are  $-2.27$ ,  $-2.81$ , and  $-6.48$  meV, respectively. As shown in Ref. 12, the LJ potential works well as a "universal" functional form for describing the binding energies in a number of carbon systems (solid  $C_{60}$ , graphite) at zero pressure. On the other hand, pressures up to 100 GPa and interlayer separations down to 1.5 Å have been treated in the LDA-based Morse potential<sup>16</sup>; we note that no intramolecular relaxation was allowed in this DFT modeling. Note that for the case studied in this paper, the shortest interatomic distance is at least larger than 2.3 Å, far from the point that a transition to a covalent bond may take place.

**Table I.** Model parameters for LJ potential.

Parameter source	$A$ ( $J \cdot m^6$ )	$\sigma$ (Å)	$y_0$
LJ1 <sup>14</sup>	$24.3 \times 10^{-79}$	1.42	2.7
LJ2 <sup>15</sup>	$32 \times 10^{-79}$	1.42	2.742

A further comparison of these two pairwise potentials has been conducted by Qian et al.<sup>17</sup> They computed the EOS for graphite with these two models by neglecting the in-plane relaxation effects. The results were compared with experimental data by Zhao and Spain<sup>18</sup> (referred to as EXP1) and by Hanfland et al.<sup>19</sup> (referred to as EXP2), and with the *ab initio* treatment (which included in-plane relaxation and treated an infinite crystal) by Boettger.<sup>20</sup> The comparison shows the nonphysical behavior of the LJ model in the repulsive region.

In this paper we have further verified this by computing the isothermal compressibility of the system based on these models. The compressibility is defined as  $\kappa = -\partial(\log V)/\partial P$ . Under ambient pressure, the computed compressibility from LJ1, LDA-based Morse, and Boettger's model are, respectively, 0.032, 0.023, and 0.024  $\text{GPa}^{-1}$ ; from EXP2, the reported compressibility of graphite under ambient pressure is 0.030  $\text{GPa}^{-1}$ . At a relative volume of 0.9, we obtain 0.008, 0.013, and 0.012  $\text{GPa}^{-1}$ , respectively, from the LJ1, LDA, and Boettger LDA-EOS models. And at a relative volume of 0.85, the computed compressibilities from the LJ1, LDA, and Boettger LDA-EOS models are 0.004, 0.01, and 0.009  $\text{GPa}^{-1}$ . These comparisons demonstrate the overly repulsive (inverse  $r^{12}$ ) LJ potential at short interlayer spacing and overly attractive Morse potential at zero pressure for graphite.

### 3. MD SIMULATIONS

The effect of interlayer potential on the bending of a MWCNT can be illustrated from MD simulations. We have used two sets of models for the interlayer potential: one model uses LJ1 regardless of the interatomic distance, the other model uses LJ1 when the interatomic distance is greater than 3.0 Å and the Morse potential for interatomic distances less than 2.9 Å, with the transition region handled by spline fitting. For the comparison of *c* axis compressibility we described above, this model yields the same result as LJ1 at zero pressure, converting to the LDA model at this transition region (3.0 to 2.9 Å). In the case of a relative volume of 0.85, it gives the same result as LDA.

The covalent (intralayer) bonding interaction is modeled with the Tersoff-Brenner potential.<sup>21</sup> The CNTs that are considered are nested (*n, n*) tubes, with *n* = 5, 10, and 15. The number of shells ranges from 1 to 3. The numbers of atoms for these CNTs are, respectively, 1250, 3750, and 7500. The lengths of all of the MWCNTs are 15.37 nm. Bending is applied at 0.25°/step increment on both ends of the MWCNTs. The atoms on the perimeter at each end are fixed in a perfect circle. The problem is solved as a quasi-static problem, that is, the equilibrium solution is obtained for each incremental step of loading. Shown in Figure 1 are the final deformation patterns of CNTs after 150 steps, from single-walled to three-walled CNT.

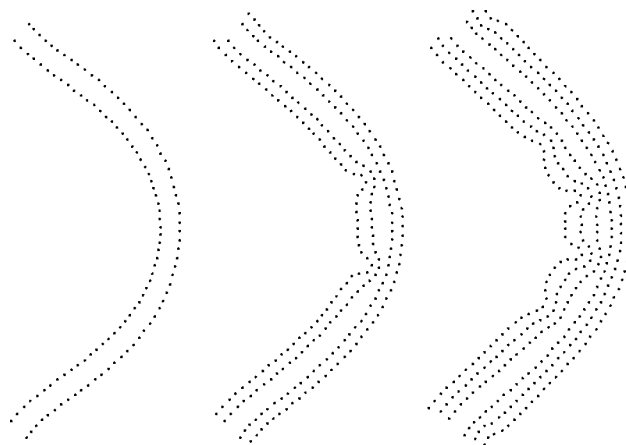


**Fig. 1.** MD simulation on bending and buckling pattern of one-, two-, and three-walled carbon nanotubes (starting from a (5,5) single-walled carbon nanotube).

An interesting transition in the response to this bending is observed in this simulation. First, the tube does not buckle in the case of the (5,5) single-walled CNT. In contrast, there are two points of local buckling for the two-walled NT. For the three-walled CNT, the number of buckling points increases to three, and the “rippling mode” develops. The rippling pattern from this simulation is similar to the ones shown by Poncharal et al.<sup>10</sup> and earlier by Ruoff and Hickman.<sup>22</sup>

The MD simulation results suggest there are competing factors influencing the final deformation pattern: the structural rigidity of the tube versus buckling due to pure bending and large compression. The single-walled (5,5) CNT can be considered as a thin beam since the aspect ratio is approximately 25. Because it has a very small radius of 0.7 nm, a buckling pattern does not occur under the external bending load. However, when nested with a (10,10) tube to form a two-walled CNT, the (10,10) starts to buckle because it has a larger radius and therefore is more compliant in the radial direction under bending. Figure 2 shows the buckling of a single (10,10) CNT



**Fig. 2.** The local buckling mode in the bending of a (10,10) carbon nanotube.

without the inner (5,5) tube. This brings the shells from two different CNTs into closer contact at the buckling point. As the radius of the MWCNT increases (three-shelled MWCNTs), the compressive strain increases for the same bending angle.

For the MWCNTs, the source of local buckling is therefore due to compression. It is thus certain that the bending angle that is needed to achieve a “rippling” mode decreases as the radius of the MWCNT increases, and that this mode is mainly dominated by partial release of a buildup in compressive stress. The role of the interlayer potential is to prevent the buckling of the outer layer from further developing when two layers are in close contact. We further verified this hypothesis by looking at the final geometry of the local buckling mode as shown in Figure 3. The closest interatomic distances corresponding to LJ and our model are, respectively, 2.7 Å and 2.3 Å.

We investigated the potential energy of the system (this includes both the bonded and the nonbonded energy) as a function of the bending angle as shown in Figure 4. Buckling starts to develop at a bending angle of approximately 35°. As Figure 4 shows, no noticeable difference is found between the two interlayer potential models up to this bending angle. In terms of the angle at the onset of buckling, and the observed buckling pattern and energy at that angle, the LJ and LDA models give exactly identical results because the interlayer separation is greater than 3.0 Å. After the buckling further develops, the LJ model curve deviates from our model and yields a binding energy higher than that of our model. The overly repulsive behavior in the buckling regions thus also influences the computed buckling geometry. As a brief summary, the LJ model probably overestimates the bending stiffness in the post-buckling stage (based on the known EOS of graphite as discussed above), and this can be corrected with the model proposed in this paper.

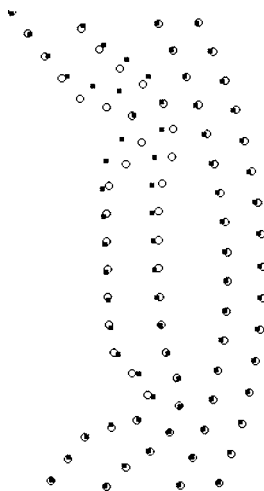


**Fig. 3.** Comparison of the buckling mode in the local area corresponding to the case of the two-walled nanotube shown in Figure 1. Open circles correspond to the case using LDA Morse potential; filled boxes are from the case using LJ potentials.

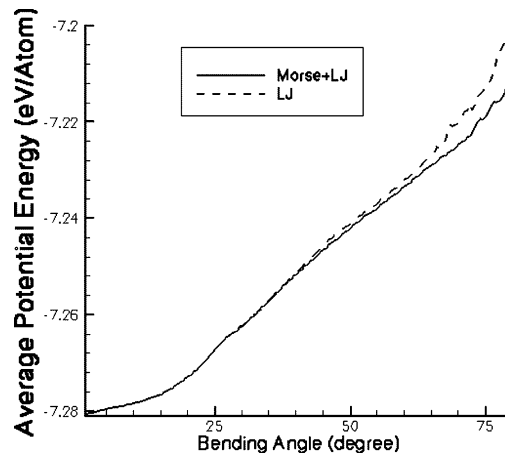


**Fig. 4.** Comparison of the average energy of the two-walled CNT as a function of the bending angle.

#### 4. EFFICIENT COMPUTATIONAL METHOD FOR EVALUATION OF INTERLAYER POTENTIAL

Even with the interlayer (pairwise) potential model that correctly accounts for the effect of interatomic distance, implementing it for MWCNTs with a large number of atoms can still be difficult. Unlike the covalent bond potential that is short ranged, a large number of pairwise interactions with neighboring atoms must be included to correctly evaluate the nonbonded potential. One way of computing this interaction is by discrete summation,

$$\phi = \sum_{\alpha} \sum_{\beta \neq \alpha} \phi(r_{\alpha\beta}) \quad (3)$$

where  $r_{\alpha\beta} = |x_{\alpha} - x_{\beta}|$  and  $\mathbf{x}$  are the spatial coordinates of the atom.

A second way of evaluating the interlayer potential is by using an analytical method. By distribution of the charges, the discrete summation in Eq. (3) is replaced with a continuous integral,

$$\phi = \int_{\Omega_{\alpha}} \int_{\Omega_{\beta}} n_{\alpha} n_{\beta} \phi(r_{\alpha\beta}) d\Omega_{\alpha} d\Omega_{\beta} \quad (4)$$

where  $n_{\alpha}$  and  $n_{\beta}$  are the surface density of the atoms. The approach has been used in deriving analytical expressions of the binding energies for various systems composed of carbon atoms.<sup>12, 23</sup> The restriction is that the shape of the “molecule” (such as the graphene sheet, the C<sub>60</sub> molecule, the carbon nanotube) must be well defined to evaluate the integral analytically. Therefore, it is mostly applicable to highly symmetrical structures that are fully relaxed. Otherwise, numerical quadrature must be applied for irregular surfaces.

The validity of these two different approaches is related to the electron distribution, as noted by Girifalco et al.<sup>12</sup> In particular, the discrete summation is not necessarily more accurate in all of the cases, particularly when the C nuclei do not lie exactly in the center of the electron distribution, as is the case for CNTs.

Equation (4) can be further extended by introduction of a computational grid to interpolate the atom positions. A powerful tool for approximating the smooth surface for CNT is the meshfree method.<sup>13, 24–28</sup> The meshfree method is essentially a *moving least-squares* type of interpolation. For a survey of meshfree and particle methods and their applications, please see Ref. 29. In addition, two special journal issues<sup>30, 31</sup> have been devoted to this topic. With the use of the meshfree shape function, the position of the atom is given as

$$x_\alpha = \sum_I N_I(X_\alpha)x_I \quad (5)$$

In the subscript in Eq. (5), we use capital letters for nodes and Greek letters for atoms. The shape function can be expressed either in terms of the material coordinates (the total Lagrangian formulation) as shown above or in terms of the spatial coordinates (the updated Lagrangian formulation).

Plugging Eq. (5) into Eq. (4) gives

$$\phi = \int_{\Omega_\alpha} \int_{\Omega_\beta} n_\alpha n_\beta \phi \times \left( \left| \sum_I N_I(X_\alpha)x_I - \sum_I N_I(X_\beta)x_I \right| \right) d\Omega_\alpha d\Omega_\beta \quad (6)$$

The solution to the molecular dynamics equation is essentially to satisfy the law of conservation of momentum. This is equivalent to the principle of virtual work,<sup>32</sup>

$$\delta W = \delta W^{\text{int}} - \delta W^{\text{ext}} + \delta W^{\text{kin}} = 0 \quad (7)$$

in which  $W^{\text{int}}$ ,  $W^{\text{ext}}$ , and  $W^{\text{kin}}$  are the internal energy, external work, and kinetic energy, respectively.

For the MWCNT system, the internal energy consists of the bonded potential  $\varphi$  and nonbonded potential  $\phi$ . Therefore, solving Eq. (7) involves the evaluation of  $\delta\phi$ , which from Eq. (6) is

$$\begin{aligned} \delta\phi &= \int_{\Omega_\alpha} \int_{\Omega_\beta} n_\alpha n_\beta \frac{\partial\phi}{\partial r_{\alpha\beta}} \\ &\cdot \left( \sum_I N_I(X_\alpha)\delta x_I - \sum_I N_I(X_\beta)\delta x_I \right) d\Omega_\alpha d\Omega_\beta \\ &= \sum_I f_I \cdot \delta x_I \end{aligned} \quad (8)$$

To evaluate Eq. (8) in the computation, we need to use numerical quadrature,

$$\begin{aligned} \delta\phi &\cong \sum_{X_\alpha^h \in \Omega_\alpha} \sum_{X_\beta^h \in \Omega_\beta} \frac{\partial\phi}{\partial r_{\alpha\beta}^h} \\ &\times \left( \sum_I N_I(X_\alpha^h)\delta x_I - \sum_I N_I(X_\beta^h)\delta x_I \right) w_\alpha^h w_\beta^h \\ &= \sum_I f_I^h \cdot \delta x_I \end{aligned} \quad (9)$$

The computational saving gained with Eq. (9) has two aspects: the original discrete summation over the atoms

is now replaced by discrete summation over the quadrature points, which can require far less computation. The interatomic forces are thus replaced by the nodal internal forces. The equilibrium is solved in terms of the computational nodes rather than each atom. Therefore, the number of degrees of freedom is also reduced. We note that this approach also must be applied to the bonded potentials to make the whole formulation consistent. The details of the treatment will be described in a future paper. Note that a similar continuum treatment for carbon nanotube structure has been proposed in Refs. 33–35. The major difference is that no concept of stress is involved in the proposed method.

## 5. SAMPLE PROBLEMS AND COMPARISON WITH EXPERIMENTS

In the following, we present some simulation results on the bending of MWCNTs. Similar to the approach used in MD, we apply the bending angle incrementally on the two ends of the tube and solve for equilibrium at each incremental step. Since the problem is treated as a quasi-static case, temperature and inertia effects are not accounted for in these simulations. The equilibrium configurations are obtained with the conjugate gradient (CG) method.

The first example is motivated by the work by Iijima et al.,<sup>36</sup> in which they observed the collapse of the cross section in the middle of the MWCNT when it is subjected to bending. In our simulation, we computed the bending of a five-walled CNT. The nested tubes, starting from the outermost shell, are (55,55), (50,50), (45,45), (40,40), and (35,35). The tube length is 32 nm. This geometry was chosen because of its similarity to the experimentally observed buckled MWCNT (Fig. 1c in Ref. 36). The original MD system has approximately 55,680 atoms, which are replaced with 3600 computational particles by the approach described in Section 5. A bending angle in increments of 0.25° is imposed for each step for a total of 100 steps.

Shown in Figure 5 is the cross-sectional shape of the tube during the course of bending. As can be seen, a rippling mode starts to develop on the compressively loaded side of the MWCNT in the initial stages of loading.

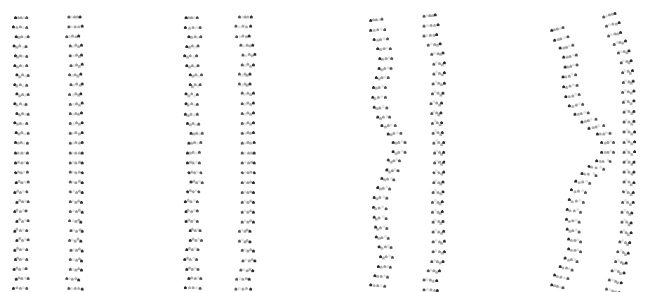


Fig. 5. Buckling of a five-walled CNT.

The strain energy accumulates until structural instability occurs as the total bending angle approaches a critical value of  $10^\circ$ . The rippling mode is then switched to a single buckling point in the middle due to the strain release mechanism, which closely resembles the experimental observation.

Ruoff and his colleagues have also conducted an interesting experiment on the mechanical deformation of MWCNTs. The polymer polyvinylformal (Formvar) has a thermal distortion temperature of  $\sim 70^\circ\text{C}$ . This polymer is used as a thin support film for TEM grids. Often, an additional support film is deposited on top, and the Formvar is removed. However, in our work we deposited MWCNTs on thin Formvar films on TEM grids and then briefly heated (for a few seconds) this thin film with a hot soldering gun tip held a few centimeters from the film. This would cause the film to thermally distort and to compressively load the MWCNTs on top of the film.<sup>22</sup> For the work reported here, we varied this procedure to embed the MWCNTs directly in the thin Formvar film. Formvar in solvent was mixed with arc-grown MWCNTs and then deposited in the standard way on water. The solvent dried, leaving MWCNTs embedded in a Formvar film  $\sim 50$  to  $100$  nm thick, which was then placed on standard TEM grids and heated briefly as described above. The MWCNT shown in Figure 6 was buckled as a consequence of the thermal distortion of this composite film.

As indicated from the MD simulations described in Section 4, the single buckling pattern is not the only mode that may take place. The second set of simulations was carried out based on the experiment described above by Ruoff et al.<sup>22</sup> A 15-walled MWCNT is considered, in which the outermost shell is a (140,140) nanotube and all inner shells are of the  $(n,n)$  type; from the outermost shell,  $n$  reduces by 5 for every layer. The length of the tube is 90 nm and the original MD system contains  $\sim 3$  million atoms. This is replaced with a system of 27,450 particles. The same loading increment as for the case of the five-walled carbon nanotube described above is applied and imposed for 50 steps. In Figure 6 is a side-by-side comparison showing the evolution of the computed buckling mode versus the experimental TEM image. After the bending load step was completed we released the load. We found that the accumulated deformation could be fully recovered. The simulation shows that the MWCNT is a remarkably resilient material.

It should be noted that we have not included here the surrounding Formvar medium, which has a Young's modulus in the bulk of  $\sim 3$  GPa, in the simulation. This is a subject for future study.

## 6. CONCLUSIONS

A realistic treatment of the interlayer potential in a MWCNT system is presented. We emphasize the unsuitability of the LJ "6-12" potential, which is far too

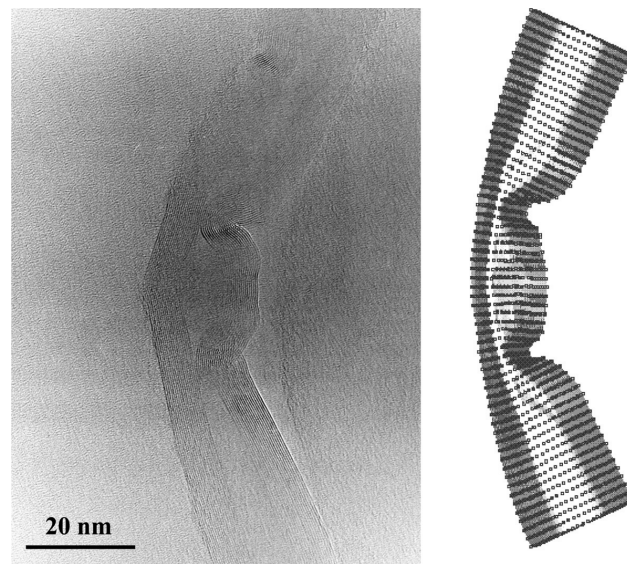


**Fig. 6.** Comparison of bending of MWCNT (left). TEM image of a bent MWCNT. (Right) Simulation of bending of a 15-walled CNT.

repulsive at small interlayer separation, and replace this repulsive wall with what we believe is a more realistic potential based on LDA calculations. A comparison of this interlayer potential with high-pressure experimental data for graphite supports this treatment. MD simulations are used to study the functional dependence on the number of layers; a transition from single buckling (an individual CNT) to the rippling mode (for MWCNTs) was observed. A simple continuum method is presented for the efficient evaluation of interlayer and intralayer bonding. Comparison with several experiments that showed images of compressively loaded MWCNTs is given. The results presented are relevant to applications involving local buckling of MWCNTs.

**Acknowledgments:** R. S. R. gratefully acknowledges the grant support from the NASA Langley Research Center for Computational Materials: Nanotechnology Modeling and Simulation Program, the NASA University Research, Engineering and Technology Institute on Bio Inspired Materials (BIMat), under award NCC-1-02037, and the Office of Naval Research Mechanics of Nanostructures grant under award N000140210870. The work of D. Q. has also been supported by the Ohio Board of Regents, the Tull Family Endowment, and the Dissertation Year Fellowship from Northwestern University while he was conducting his Ph.D. study. R. S. R. and W. K. L., for some of the work described here, have been supported by grants from the National Science Foundation.

## References and Notes

1. S. Iijima, *Nature* 354, 56 (1991).
2. Y. Saito, T. Yoshikawa, S. Bandow, M. Tomita, and T. Hayashi, *Phys. Rev. B* 48, 1907 (1993).

3. O. Zhou, R. M. Fleming, D. W. Murphy, C. H. Chen, R. C. Haddon, A. P. Ramirez, and S. H. Glarum, *Science* 263, 1744 (1994).
4. M. F. Yu, B. I. Yakobson, and R. S. Ruoff, *J. Phys. Chem. B* 104, 8764 (2000).
5. J. Cumings and A. Zettl, *Science* 289, 602 (2000).
6. D. Qian, G. J. Wagner, W. K. Liu, M. F. Yu, and R. S. Ruoff, *Appl. Mech. Rev.* 55, 495 (2002).
7. B. I. Yakobson, C. J. Brabec, and J. Bernholc, *Phys. Rev. Lett.* 76, 2511 (1996).
8. J. Bernholc, C. Brabec, M. B. Nardelli, A. Maiti, C. Roland, and B. I. Yakobson, *Appl. Phys. A* 67, 39 (1998).
9. B. I. Yakobson and P. Avouris, in *Carbon Nanotubes* (2001), Vol. 80, pp. 287–327.
10. P. Poncharal, Z. L. Wang, D. Ugarte, and W. A. de Heer, *Science* 283, 1513 (1999).
11. D. Srivastava, D. W. Brenner, J. D. Schall, K. D. Ausman, M. F. Yu, and R. S. Ruoff, *J. Phys. Chem. B* 103, 4330 (1999).
12. L. A. Girifalco, M. Hodak, and R. S. Lee, *Phys. Rev. B* 62, 13104 (2000).
13. W. K. Liu, S. Jun, and Y. F. Zhang, *Int. J. Numer. Methods Fluids* 20, 1081 (1995).
14. L. A. Girifalco and R. A. Lad, *J. Chem. Phys.* 25, 693 (1956).
15. L. A. Girifalco, *J. Phys. Chem.* 96, 858 (1992).
16. Y. Wang, D. Tomanek, and G. F. Bertsch, *Phys. Rev. B* 44, 6562 (1991).
17. D. Qian, W. K. Liu, and R. S. Ruoff, *J. Phys. Chem. B* 105, 10753 (2001).
18. Y. X. Zhao and I. L. Spain, *Phys. Rev. B* 40, 993 (1989).
19. M. Hanfland, H. Beister, and K. Syassen, *Phys. Rev. B* 39, 12598 (1989).
20. J. C. Boettger, *Phys. Rev. B* 55, 11202 (1997).
21. D. W. Brenner, *Phys. Rev. B* 42, 9458 (1990).
22. S. Subramoney, R. S. Ruoff, R. Laduca, and K. Parvin, in *Mechanical Deformation of Multi-walled Carbon Nanotubes* (1996), pp. 728–739.
23. R. S. Ruoff and A. P. Hickman, *J. Phys. Chem.* 97, 2494 (1993).
24. W. K. Liu, S. Jun, S. F. Li, J. Adey, and T. Belytschko, *Int. J. Numer. Methods Eng.* 38, 1655 (1995).
25. W. K. Liu, Y. J. Chen, R. A. Uras, and C. T. Chang, *Comput. Methods Appl. Mech. Eng.* 139, 91 (1996).
26. W. K. Liu, Y. Chen, C. T. Chang, and T. Belytschko, *Comput. Mech.* 18, 73 (1996).
27. W. K. Liu, S. Jun, D. T. Sihling, Y. J. Chen, and W. Hao, *Int. J. Numer. Methods Fluids* 24, 1391 (1997).
28. W. K. Liu, S. F. Li, and T. Belytschko, *Comput. Methods Appl. Mech. Eng.* 143, 113 (1997).
29. S. F. Li and W. K. Liu, *Appl. Mech. Rev.* 55, 1 (2002).
30. W. K. Liu, T. Belytschko, and J. T. Oden, *Computer Methods in Applied Mechanics and Engineering*, North-Holland, Amsterdam (1996), Vol. 139.
31. J. S. Chen and W. K. Liu, Editors, *Computational Mechanics*, Springer-Verlag, Berlin (2000), Vol. 25.
32. T. Belytschko, W. K. Liu, and B. Moran, *Nonlinear Finite Elements for Continua and Structures*, Wiley, New York (2000).
33. P. Zhang, Y. Huang, P. H. Geubelle, P. A. Klein, and K. C. Hwang, *Int. J. Solids Struct.* 39, 3893 (2002).
34. P. Zhang, Y. Huang, H. Gao, and K. C. Hwang, *J. Appl. Mech.* 69, 454 (2002).
35. M. Arroyo and T. Belytschko, *J. Mech. Phys. Solids* 50, 1941 (2002).
36. S. Iijima, C. Brabec, A. Maiti, and J. Bernholc, *J. Chem. Phys.* 104, 2089 (1996).

Received: 23 July 2002. Revised/Accepted: 14 February 2003.